ICAS 2016
30th Congress of the International Council of the Aeronautical Sciences
DCC, Daejeon, Korea ; September 25-30, 2016

PID TUNING FOR MULTI-CHANNEL STRUCTURAL FATIGUE TESTING SYSTEM

Hongwei Zhao, Shihui Duan and Jianmin Feng
Aircraft Strength Research Institute of China
zhw_zhaohongwei@sina.com

Keywords: *aircraft; multi-channel; control; PID;*

Abstract

A proportion-integration-differentiation (PID) controller is a generic control loop feedback mechanism widely used in multi-channel aircraft structural fatigue test. The PID parameter is obtained by test setup method in which PID is tuned after the test setup is actually performed, so that the tuning period becomes overlong. And the dynamic characteristic of mechanical and hydraulic equipment isn't considered as a crucial factor to decrease working capability of loading equipment. at the same time, there is coupling effect among channels, which lower control accuracy. For this, based on multi-channel fatigue test of cantilever beam, the coupling mathematics model of testing system is presented and linearized reasonably. The basic procedure of a multi-channel fatigue test is analyzed systematically. The PID parameter of every channel is simulated by stability margin and bandwidth analysis. The dynamic characteristic of hydraulic equipment and test article are analyzed. Finally, a double channel fatigue test of cantilever beam is implemented. The results of simulation and test show that the new method is effective. This method not only has the ability to predict PID parameter rapidly and the dynamic characteristic of test equipment, but it can also reduce effectively the control errors.

1 Introduce

Full-scale structural testing of aircraft structures has been and still is the task of the aircraft industry when new aircrafts are developed. In recent years, as China has been developing the aviation industry and the research has been entering into a new stage, the requirements of aircraft structure fatigue test become increasing. Aircraft structure fatigue test employ multi-channel coordinated loading control system to drive the hydraulic system to apply load spectrum to aircraft structure. Fatigue test system adopts PID control. Namely, the testing system calculates the control quantity by PID algorithm based on system error. Currently, the tuning to PID of test system is completed using experience after test setup installation, so that the PID prediction is difficult to implement to increase tuning time to impact test cycle. And dynamic characteristics of the mechanical and hydraulic equipment have not considered fully, and the capacity of loading equipment is not enough. Worse, the coupling phenomenon among the actuator cylinders has been occurring.

Due to the above problems, aircraft structural test cannot be run smoothly, and the test results cycle are affected seriously. For this, in 2010, Eenkhoorn N.C. of Delft University of Technology in the Netherlands has carried out the PID simulation in single channel structural fatigue[1]. Despite controller, hydraulic system and test article are coupled, Dr E has not yet researched multi-channel test system, and the methods have not been applied

in engineering. In 2012, Xiasheng Sun of aircraft strength research institute of China have studied the PID simulation of control channel for MTS control system[2]. This method is just focus on the controller, not the hydraulic system and test article. In 2015, Shihui Duan of aircraft strength research institute of China has simulated PID parameter of the cantilever beam structure test system[3]. The control system, hydraulic system and mechanical system are coupled to tune PID of the testing system. This method is applied to structural tests. Unfortunately, the method is based on single channel test system.

The above researches are almost related to single channel fatigue test system, so the multi-channel test system research is increasingly important. Therefore, in 2010, professor Huaihai Chen of nanjing university of aeronautics and astronautics has studied variable parameter PID control method for multiple input multiple output random vibration test[4]. The basic procedure of multiple input multiple output random vibration test is analyzed systematically in the article. A definition of control error under logarithmic coordinates is provided, a new PID control strategy is introduced into the control algorithm. But the method does not take into account the hydraulic system and test article effecting to PID and control error. In 2013, professor Jianyu Zhao of jinan university has studied multi-channel coordinated loading control method[5]. This approach is based on neural network algorithm. But it is not involving the hydraulic system and test article of testing system. The other researching refer to the hydraulic system[6~7] or control system[8~10] or developing to control algorithm[11~14] or the coupling simulation between two systems[15~17] or the coupling simulation among the hydraulic systems, control system and test article[18~19]. Currently, The research about single-channel fatigue test is more than multi-channel test system's. So the thesis considers multi-channel cantilever beam structure fatigue test system as the research object. The mathematical model of subsystem is presented. The coupling characteristic of test system is analyzed. The PID parameter of every channel is simulated to compensate coupling effect among channels. Dynamic characteristic of hydraulic system is described to improve capacity to testing system.

2 Modelling Theory

2.1 Modelling of servo-valve

The structure of the force feedback two stage servo valve is shown in Fig. 1. The valve keeps a good linear, due to Armature and Baffle working in the zero position.

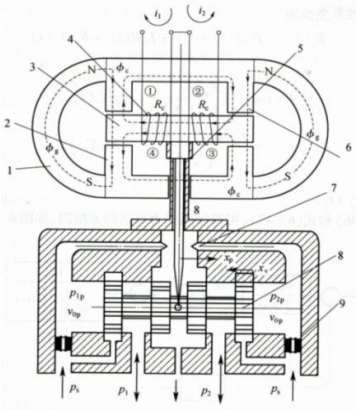

1. Magnet 2. Lower guide magnet 3. Armature 4. Coil 5. Spring tube 6. Upper guide magnet 7. Nozzle 8. Slide valve 9. Fixed orifice

Fig. 1 Principle diagram of servo vavle

There is a large number of parameters in the structure of servo valve, so the dynamic characteristic of armature motor and nozzle flapper is ignored. The paper just researches dynamic characteristic of spool[20~21]. Its dynamic behavior is described by a second-order model:

$$\frac{1}{\omega_{sv}^2}\ddot{x}_v + \frac{2\xi_{sv}}{\omega_{sv}}\dot{x}_v + x_v = k_{sv}I_{sv} \tag{1}$$

where k_{sv} is valve gain; ω_{sv} is eigenfrequency of the valve; ξ_{sv} is rate of damping coefficient; x_v is position of valve; I_{sv} is valve control input.

Equations 1 is converted to transfer function by

Laplasse transform from valve control input to spool position output, as Equations 2 shown:

$$G_1(s)=\frac{X_v(s)}{I(s)}=\frac{k_{sv}\omega_{sv}^2}{s^2+2\omega_{sv}\xi_{sv}s+\omega_{sv}^2} \tag{2}$$

2.2 Modelling of hydraulic actuator

The transfer function of hydraulic actuator is deduced using flow equation of valve, hydraulic spring stiffness equation of actuator, flow continuity equation of actuator and force balance equation of piston[21~23]. Derivation process is divided into two steps: spool moving to the left and right.

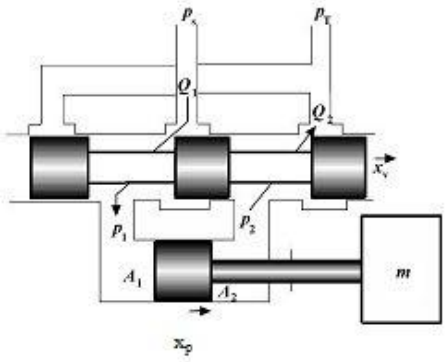

Fig. 2 structural diagram of Valve-controlled cylinder

As Fig. 2 shown, when spool position x_v>0, the spool will move to the right. The flow rate of actuator is equation 3.

$$\alpha=\frac{Q_2}{Q_1}=\frac{A_2}{A_1} \tag{3}$$

where α is flow rate($0.5\leqq\alpha\leqq1$); A_1 is piston area of rear chamber; A_2 is anterior chamber.

The load pressure can be written as equation 4.

$$\begin{cases} P_L=\dfrac{F}{A_{01}}=\dfrac{P_1-\alpha P_2}{\alpha(2-\alpha)} \\ A_{01}=\alpha A_1+(1-\alpha)A_2 \end{cases} \tag{4}$$

where F is external load; A_{01} is equivalent confined area of piston when the spool will move to the right; P_L is load pressure.

The load flow is defined as equation 5.

$$q_L=\frac{Q_1+Q_2}{2} \tag{5}$$

where q_L is load flow.

Combine equation 3,4,5 to obtain equation 6.

$$\begin{cases} q_L=\varepsilon_1\omega x_v\sqrt{\dfrac{1}{\rho}\left[P_s-\alpha(2-\alpha)P_L\right]} \\ \varepsilon_1=\sqrt{\dfrac{(1+\alpha)^2}{2(1+\alpha^3)}} \end{cases} \tag{6}$$

where ε_1 is rate; ω is area gradient of valve orifice; P_S is supply pressure; ρ is oil density.

The equation 6 can be linearized to gain equation 7 by Taylor series.

$$\begin{cases} q_L=k_{q1}x_v-k_{c1}P_L \\ k_{q1}=\varepsilon_1 C_d\omega\sqrt{\dfrac{1}{\rho}\left[P_s-\alpha(2-\alpha)P_L\right]} \\ k_{c1}=\dfrac{\varepsilon_1\alpha(2-\alpha)C_d\omega x_v}{\sqrt{\rho\left[P_s-\alpha(2-\alpha)P\right]}} \end{cases} \tag{7}$$

where k_{q1} is zero position flow gain when the spool will move to the right; k_{c1} is flow-pressure coefficient; C_d is flow coefficient;

When x_v<0, the spool will move to the left, in the same way, equation 8 is obtained.

$$\begin{cases} q_L=k_{q2}x_v-k_{c2}P_L \\ k_{q2}=\varepsilon_2 C_d\omega\sqrt{\dfrac{1}{\rho}\left[P_s-\left(\dfrac{1}{\alpha}-1+\alpha^2\right)P_L\right]} \\ k_{c2}=\dfrac{\varepsilon_2\left(\dfrac{1}{\alpha}-1+\alpha^2\right)C_d\omega x_v}{2\sqrt{\rho\left[P_s-\left(\dfrac{1}{\alpha}-1+\alpha^2\right)P_L\right]}} \\ \varepsilon_2=\sqrt{\dfrac{\alpha(1+\alpha)^2}{2(1+\alpha^3)}} \\ A_{02}=\alpha A_2+(1-\alpha)A_1 \end{cases} \tag{8}$$

where k_{q2} is zero position flow gain when the spool will move to the left; ε_2 is rate; A_{01} is equivalent confined area of piston when the spool will move to the left.

when hydraulic actuator system has its lowest eigenfrequency, its damping ratio is minimum, and the stability is worst, and the hydraulic spring stiffness is minimum.

The hydraulic spring stiffness is generated by the compressibility of oil, when the chambers are seal fully. Assuming that the piston rod length is x, equation 9 is gained using Hooke's law.

$$K_{h1} = \frac{F_1}{x_p} = \frac{\Delta p_1}{x_p} \tag{9}$$

where k_{h1} is hydraulic spring stiffness; F_1 is hydraulic spring force of rear chamber; Δp_1 is pressure change of rear chamber; x_p is piston position.

The bulk modulus β_e of rear chamber is described as equation 10.

$$\beta_e = \frac{\Delta p_1}{\Delta V_1 / V_1} \tag{10}$$

Combine equation 9 and 10 to obtain equation 11.

$$K_{h1} = \frac{\beta_e A_1^2}{V_1} \tag{11}$$

In the same way, equation 12 is gained.

$$K_{h2} = \frac{\beta_e A_2^2}{V_2} \tag{12}$$

The hydraulic spring stiffness is described as equation 13 for the whole hydraulic actuator system.

$$K_h = \frac{\beta_e A_1^2}{V_1} + \frac{\beta_e A_2^2}{V_2} \tag{13}$$

When K_h is minimum, equation 14 is obtained.

$$\frac{A_1^2}{V_1} = \frac{A_2^2}{V_2} \tag{14}$$

Finally, when hydraulic actuator system has its lowest eigenfrequency, piston position x_p is described by equation 15.

$$x_p = \frac{L}{1+\alpha} \tag{15}$$

Where L is stroke of actuator.

Piston operation is divided into two steps: flowing into rear chamber, flowing out anterior chamber; flowing out rear chamber, flowing into anterior chamber.

When oil flows into rear chamber, equation 16 is obtained.

$$q_L = \frac{Q_1 + Q_2}{2} = \frac{A_1 + A_2}{2}\dot{y} + \frac{V_1}{2\beta_e}\dot{P}_1 - \frac{V_2}{2\beta_e}\dot{P}_2 \tag{16}$$

And total volume of actuator V_o is described as equation 17.

$$V_0 = (A_1 + \alpha A_2)\frac{L}{1+\alpha} \tag{17}$$

At last, equation 18 is gained.

$$\begin{cases} q_L = A_e \dot{x}_p + \dfrac{h_1 V_0}{2\beta_e}\dot{P}_L \\ A_e = \dfrac{A_1 + A_2}{2} \\ h_1 = \dfrac{\alpha(2-\alpha)}{1+\alpha^2} + \dfrac{\alpha(2-\alpha)(1-\alpha)}{10(1+\alpha^2-\alpha)} \end{cases} \tag{18}$$

where A_e is average area of piston; h1 is proportional coefficient.

In the same way, When oil flows out rear chamber, equation 19 is obtained.

$$\begin{cases} q_L = A_e \dot{x}_p + \dfrac{h_2 V_0}{2\beta_e}\dot{P}_L \\ h_2 = \dfrac{(1+\alpha^2-\alpha)}{1+\alpha^2} + \dfrac{(\alpha-1)}{10} \end{cases} \tag{19}$$

For force balance equation of piston, When oil flows into rear chamber, equation 20 is obtained.

$$F = A_{01} P_L = m\ddot{x}_p \tag{20}$$

When oil flows into rear chamber, equation 21 is obtained.

$$F = A_{02} P_L = m\ddot{x}_p \tag{21}$$

Not considering external load, transfer function of actuator is gained, as equation 22 shown.

$$G_2(s) = \frac{F(s)}{X_v(s)} = \frac{k_{sv}}{\frac{h_1 V_0 m}{2\beta_e A_{01}} s^3 + m k_c \sqrt{\frac{h_1}{h_2 A_{01} A_{02}}} s^2 + A_e s} \frac{1}{ms^2} \tag{22}$$

where F(s) is output loading; m is mass of dynamic section.

2.3 Modelling of test article

To couple test article with hydraulic system, the test article state space model is presented. Under physical coordinates, the dynamic model of test article is written as equation 23.

$$M\ddot{w}(t) + C\dot{w}(t) + Kw(t) = F_e(t) \tag{23}$$

where w(t) is displacement vector of test article; Fe(t) is external force; M is mass matrix; K is

Stiffness matrix; C is damping matrix;

By introducing state space model, the number of states is increased by equation 23, which increases the computational time. To decrease the number of states it is possible to perform a modal analysis and obtain a state space representation using eigenfrequencies and eigenvectors, which is called a normalized state space[24]. To simplify the complexity of the model and reduce computational time, reduction of the normalized state space model can be applied. equation 24 is obtained.

$$\begin{cases} \dot{z} = \begin{bmatrix} \dot{x} \\ \ddot{x} \end{bmatrix} = \begin{pmatrix} 0 & I \\ -\Omega_m^2 & -2\Omega_m^2\zeta_m \end{pmatrix} \begin{bmatrix} x \\ \dot{x} \end{bmatrix} + \begin{bmatrix} 0 \\ -r(t) \end{bmatrix} [u] \\ y = \begin{pmatrix} \phi_m & 0 \\ 0 & \phi_m \end{pmatrix} \begin{bmatrix} x \\ \dot{x} \end{bmatrix} + \begin{bmatrix} 0 \\ 0 \end{bmatrix} [u] \end{cases} \tag{24}$$

where x is generalized displacement; Ω_m is eigenfrequencies matrix; ζ_m is structural damping matrix; Φ_m is mode shape vector; r(t) is input load matrix.

In fact, Ω_m, ζ_m and Φ_m are related to M, K and C which are obtained by Finite element model of test article.

The state space equation 24 can be converted into transfer function 25.

$$G_3(s) = \frac{W(s)}{F(s)} = C_{2m\times 2m}\left(sI_{2m\times 2m} - A_{2m\times 2m}\right)^{-1} B_{2m\times 1} + D_{2m\times 1} \tag{25}$$

where W(s) is displacement of loading point; F(s) is input load.

The key to study PID tuning method of multi-channel testing system is presenting to coupled mathematical model of test article. The coupling among channels is related to coupling among loading points directly.

2.4 Modelling of controller

MOOG control system which widely used in structural fatigue test is selected as controller in the paper. Block diagram of MOOG controller is shown as Fig. 3. Equation 26 is obtained by the block diagram.

$$G_4(s) = \frac{I(s)}{E(s)} = \frac{k_p s^2 + \left(293k_i + \frac{1}{2.3}k_p\right)s + \frac{293}{2.3}k_i}{s^2 + \left(293k_d + \frac{1}{2.3}\right)s} \tag{26}$$

where I(s) is control input; E(s) is control error; P is proportional gain; I is integral gain; D is damping gain.

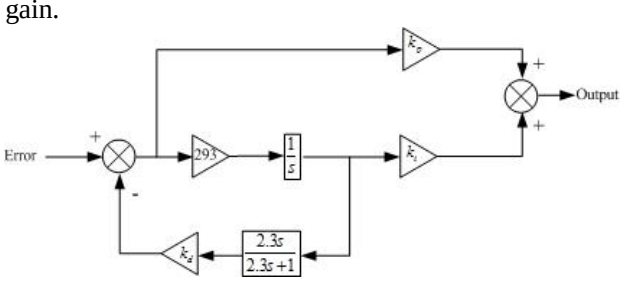

Fig. 3 Block diagram of MOOG controller

Finally, based on transfer function of each subsystem, transfer function, $G_k(s)$ for open loop system and $G_b(s)$ for closed loop system, can be gained, as equation 27 shown.

$$\begin{cases} G_k(s) = \dfrac{W(s)}{E(s)} = G_4(s)G_1(s)G_2(s)G_3(s) \\ G_b(s) = \dfrac{G_k(s)}{1+G_k(s)} \end{cases} \tag{27}$$

Equation 27 can be analyzed and simulated using stability margin analysis and bandwidth analysis. Namely, keep gain margin h>0, phase margin θ>0 and bandwidth B>10 Hz to simulate testing system. The gain and phase margin are measurement to relative stability, and bandwidth is measurement to track performance of reference signal[25].

3 Simulation and Analysis

A double-channel fatigue testing system of cantilever beam is used to verify the new mothod.

In simulation, assume that k_p=10, k_i=0.18, k_d=0.1, dynamic characteristic of controller is shown as Fig. 4.

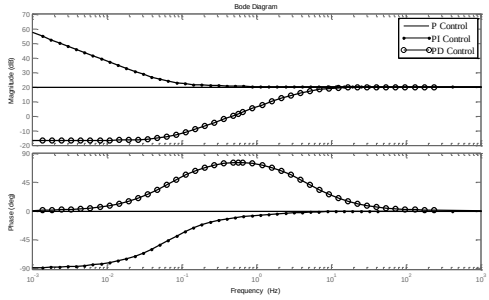

Fig. 4 Linearized frequency response of Controller

MOOG 3002B valve is selected as the simulated servo valve in the paper. Its parameters are as follows. K_{sv} =0.0625; ω_{sv} =75 Hz; ξ_{sv}=0.7063. Based on parameters and equation 2, transfer function and bode plot of 3002B valve are obtained, as equation 28 and Fig. 5 shown.

$$G_1(s) = \frac{13879}{s^2 + 666s + 222070} \tag{28}$$

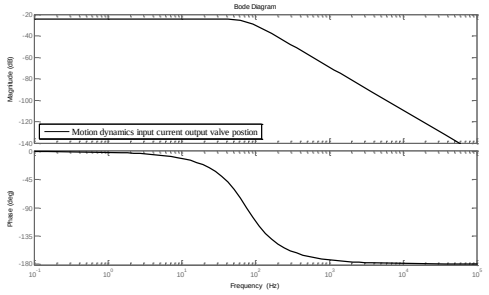

Fig. 5 Servo valve motion dynamics, between current input and position output

Hydraulic actuator contains two model. Actuator I is 2 tonnage and 300 mm stroke, actuator J is 3 tonnage and 300 mm stroke. Parameters of actuator I are as follows. A_1=0.0012 m^2 ; A_2=0.0031 m^2 ; m=13.65 Kg; for actuator J, A_1=0.0016 m^2 ; A_2=0.0044 m^2 ; m=18.5 Kg; β_e=1.3 GPa; ρ_{oil}=900 Kg/m^3; P_s=21 MPa; C_d=0.7;

Based on parameters and equation 22, transfer function and bode plot of actuator I and J can be obtained, as equation 29 and Fig. 6,7 shown.

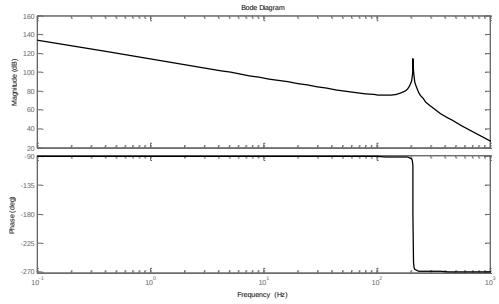

Fig. 6 Bode plot, presenting linearized frequency dependent behaviour of actuator I for a valve position input and piston position output

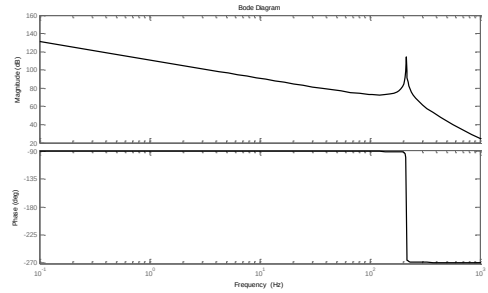

Fig. 7 Bode plot, presenting linearized frequency dependent behaviour of actuator J for a valve position input and piston position output

$$\begin{cases} G_{2,\ I}(s) = \dfrac{6729}{1.2e-9s^3 + 7.4e-9s^2 + 0.0022s} \dfrac{1}{13.65s^2} \\ G_{2,\ J}(s) = \dfrac{6647}{1.7e-9s^3 + 6.9e-9s^2 + 0.003s} \dfrac{1}{18.5s^2} \end{cases} \tag{29}$$

A two meters long cantilever beam is selected as the test article in the simulation. Its scale is 0.1×0.1×0.005 m; ρ_T=7580 Kg/m^3; I_T=2.8568×10^{-6} m^4; E=210 GPa; Midpoint and endpoint of test article is loading.

The current state space model is calculated from a finite element model using 100 elements in total, because the interest is on the low frequency depended behaviour up to 1000 Hz. As a result 200 eigenfrequencies are obtained from the eigenvalue analysis, since $M^{-1}K$ results in a 200×200 matrix. 200 Eigenfrequencies and a 200×200 eigenvector matrix is large (for our application), since fatigue testing is performed in a frequency range till 5 [Hz]. Reduction of the state space system is needed to

reduce computational time. For the reduction step, model truncation is used, taking into account the first 4 eigenmodes and eigenfrequencies of the system. This resulted in an accurate description of the system behaviour up to 100 [Hz], which is sufficient because the fatigue loading reference signal has a low frequency content. Transfer function and bode plot of test article are obtained, as equation 30 and Fig. 8 and 9 shown.

$$\begin{cases} G_{3,I}(s) = \dfrac{1.14\text{e-}13s^7 + 0.49s^6 + 84s^5 + 2\text{e}7s^4 + 1.41\text{e}9s^3 + 1.2\text{e}14s^2 + 1.41\text{e}15s + 4.11\text{e}19}{209s^7 + 4.77\text{e}7s^6 + 4.88\text{e}9s^5 + 4.12\text{e}14s^4 + 1.37\text{e}16s^3 + 4.46\text{e}20s^2 + 1.91\text{e}21s + 1.35\text{e}25} \\ G_{3,J}(s) = \dfrac{-8.5\text{e-}14s^7 - 0.1s^6 - 22s^5 - 5.8\text{e}6s^4 - 4.4\text{e}8s^3 - 4.5\text{e}13s^2 - 1.42\text{e}14s - 1.12\text{e}19}{209s^7 + 4.77\text{e}7s^6 + 4.88\text{e}9s^5 + 4.12\text{e}14s^4 + 1.37\text{e}16s^3 + 4.46\text{e}20s^2 + 1.91\text{e}21s + 1.35\text{e}25} \end{cases} \quad (30)$$

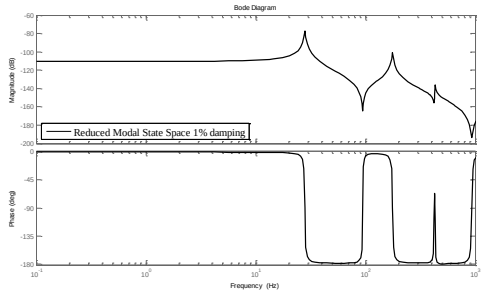

Fig. 8 Cantilever Beam bode plot for point I

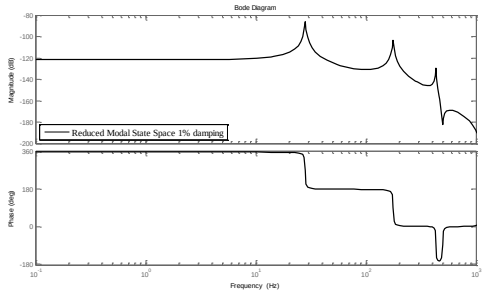

Fig. 9 Cantilever Beam bode plot for point I

Two load applied on the test article are both down, which formed a strong coupling state between two loading points. So transfer function of point I and J is relevant. PID tuning method can be used to decrease the relevance. For channel I and J, servo valve, hydraulic actuator, and test article are coupled to obtain transfer function and bode plot of controlled system, as equation 31 and Fig. 10 and 11 shown.

$$\begin{cases} G_{123,I}(s) = \dfrac{0.32\text{e}6s^7 + 7.3\text{e}11s^6 7.5\text{e}12s^5 + 6.3\text{e}17s^4 2.1\text{e}19s^3 6.86\text{e}23s^2 2.94\text{e}24s + 2\text{e}28}{1.9\text{e-}22s^{12} + 8.16\text{e-}10s^{11} + 6.87\text{e-}7s^{10} + 0.04s^9 + 26s^8 + 2.7\text{e}5s^7 + 1.8\text{e}8s^6 + 4.9\text{e}11s^5 + 2.9\text{e}14s^4 + 2.21\text{e}17s^3 + 8.31\text{e}19s^2 + 2.74\text{e}22s} \\ G_{123,J}(s) = \dfrac{0.32\text{e}6s^7 + 7.3\text{e}11s^6 7.5\text{e}12s^5 + 6.3\text{e}17s^4 2.1\text{e}19s^3 6.86\text{e}23s^2 2.94\text{e}24s + 2\text{e}28}{-1.42\text{e-}22s^{12} - 1.67\text{e-}10s^{11} - 1.48\text{e-}7s^{10} - 0.01s^9 - 7.48s^8 - 0.95\text{e}5s^7 - 0.64\text{e}8s^6 - 1.38\text{e}11s^5 - 7.73\text{e}13s^4 + 8.1\text{e}15s^3 + 2.25\text{e}19s^2 + 7.46\text{e}21s} \end{cases} \quad (31)$$

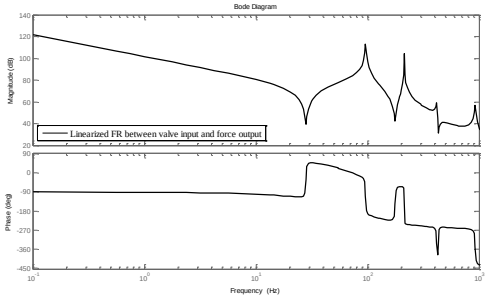

Fig. 10 Frequency response of Controlled system(I)

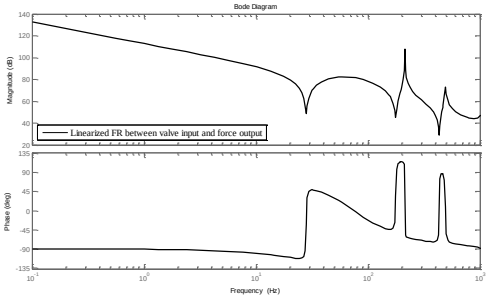

Fig. 11 Frequency response of Controlled system(J)

Based on stability margin analysis and bandwidth theory, PID parameter of fatigue testing system is tuned to reduce testing time and cost and risk.

For channel I, PID is tuned as follows. P=1.5~2.5, I=3.5~5, D=0.015~0.03. And for channel J, P=1.4~2, I=2.8~4, D=0.02~0.05. A group of parameter in the each scope is selected to obtain transfer function and bode plot of open and closed loop system, when P=2, I=4, D=0.02 for the channel I, P=1.8, I=3, D=0.04 for the channel J, as

equation 32 and Fig. 12 and 13 shown.

$$\begin{cases} G_{k,I}(s)=\dfrac{2.6s^9+6e5s^8+4e8s^7+5e12s^6+3e15s^5+5.6e18s^4+3e21s^3+2e23s^2+10e25s+4e25}{1.43e\text{-}22s^{14}+6.16e\text{-}10s^{13}+5.2e\text{-}7s^{12}+0.03s^{11}+20s^{10}+2e5s^9+1.4e8s^8+3.6e11s^7+2e14s^6+1.6e17s^5+6e19s^4+2e22s^3+1.23e23s^2} \\ G_{b,I}(s)=\dfrac{2.6s^9+6e5s^8+4e8s^7+5e12s^6+3e15s^5+5.6e18s^4+3e21s^3+2e23s^2+10e25s+4e25}{1.43e\text{-}22s^{14}+6.16e\text{-}10s^{13}+5.2e\text{-}7s^{12}+0.03s^{11}+20s^{10}+2e5s^9+1.4e8s^8+3.6e11s^7+2e14s^6+1.6e17s^5+6.6e19s^4+2e22s^3+3e23s^2+9.8e25s+4.25e25} \\ G_{k,J}(s)=\dfrac{2.3s^9+5e5s^8+3e8s^7+4.6e12s^6+2.38e15s^5+5e18s^4+2.43e21s^3+1.6e23s^2+7.2e25s+3.17e25}{-1.43e\text{-}22s^{14}-1.67e\text{-}10s^{13}-1.5e\text{-}7s^{12}-0.01s^{11}-7.6s^{10}-0.95e5s^9-0.64e8s^8-1.4e11s^7-7.9e13s^6+7.18e15s^5+2.26e19s^4+7.75e21s^3+9.08e23s^2} \\ G_{b,J}(s)=\dfrac{2.3s^9+5e5s^8+3e8s^7+4.6e12s^6+2.38e15s^5+5e18s^4+2.43e21s^3+1.6e23s^2+7.2e25s+3.17e25}{-1.43e\text{-}22s^{14}-1.67e\text{-}10s^{13}-1.5e\text{-}7s^{12}-0.01s^{11}-7.6s^{10}-0.95e5s^9-0.64e8s^8-1.4e11s^7-7.44e13s^6+9.55e15s^5+2.76e19s^4+1.02e22s^3+2.5e23s^2+7.29e25s+3.17e25} \end{cases} \quad (32)$$

As Fig. 12 shown, h=1.12 dB, θ=0.539 deg. Channel I is stable, While B=15 Hz, tracking performance of control signal is well. In the same way, As Fig. 13 shown, h=8.75 dB, θ=3.71 deg. Channel J is stable too, While B=18 Hz, tracking performance of control signal is better than channel I. In fact, due to fault tolerance to controller parameter, it is reasonable that the predicted PID is in the scope.

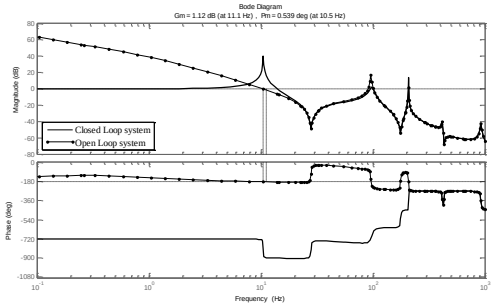

Fig. 12 Dynamic curve of channel I

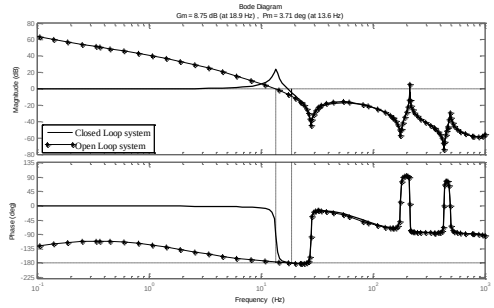

Fig. 13 Dynamic curve of channel J

4 Test and Verification

A platform of double-channels cantilever beam structural fatigue test as Fig. 14 shown, is used to verify the PID tuning method.

Fig. 14 Platform of cantilever beam fatigue test

The reference signal is sinusoidal signal in the channel I and J. The signal amplitude is 3 KN and 4.5 KN respectively, phase is zero, and frequency is 0.1 Hz.

Test result is as follows. Control error is given in method E, Sun, Zhao, and test setup method and the new method, as Fig. 15 to 24 shown. Tab. 1 shows contrasting to load error in several methods.

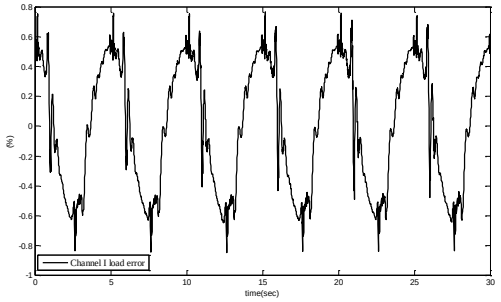

Fig. 15 Error of method E in the channel I

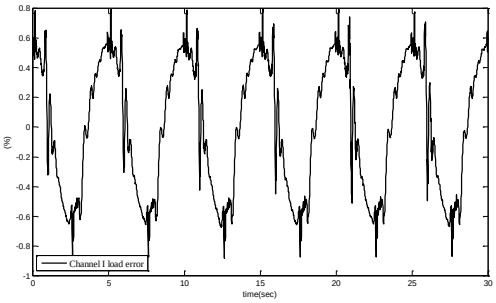

Fig. 16 Error of method Sun in the channel I

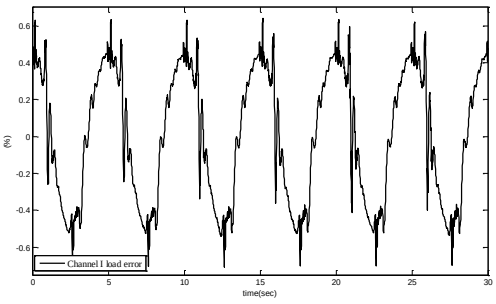

Fig. 17 Error of method Zhao in the channel I

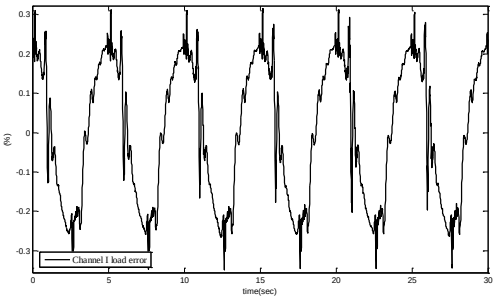

Fig. 18 Error of test setup method in the channel I

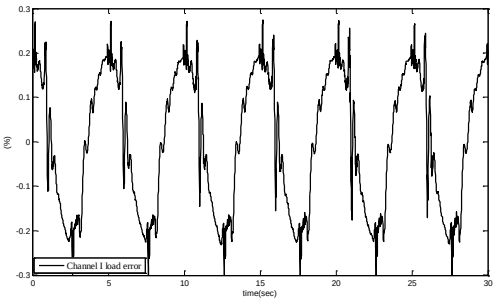

Fig. 19 Error of the new method in the channel I

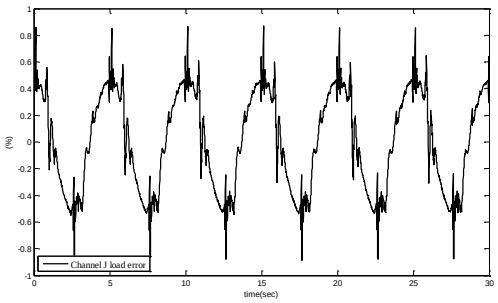

Fig. 20 Error of method E in the channel J

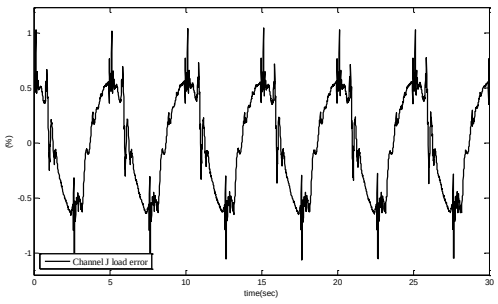

Fig. 21 Error of method Sun in the channel J

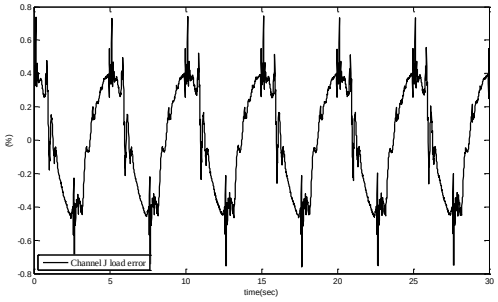

Fig. 22 Error of method Zhao in the channel J

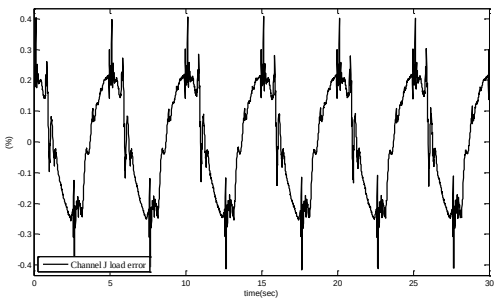

Fig. 23 Error of test setup method in the channel J

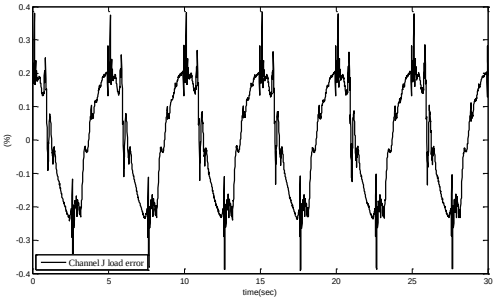

Fig. 24 Error of the new method in the channel J

Tab. 1 contrasting to load error

Error	Method E	Method Sun	Method Zhao	Test setup method	The new method
Error I	0.85%	0.9%	0.7%	0.35%	0.29%
Error I	0.93%	1.2%	0.78%	0.42%	0.37%

5 Final considerations

In first two methods, in the one hand, coupling between channels is not considered, so the control error is larger than others obviously. In the another hand, due to hydraulic system and test article coupled, the error of method E is lower than method Sun's. The error of the new method is the lowest than others. In general, PID of testing system is predicted using computational models before the certification test is actually performed in the new method.

- The testing behaviour and PID parameter of testing system is predicted using computational models before the certification test is actually performed in the new method;
- The control error of the new method is minimum in all of the methods to decrease couple affect among channels.
- The new method provide not only theoretical basis to PID tuning of multi-channel fatigue testing system, but a methodology to similar systems.

References

[1] Eenkhoorn N.C. Development of Virtual Testing Methodology for Structural Fatigue Testing Setups[D]. The Netherlands. Delft University of Technology, 2010.

[2] Huang He. Method for PID Multi-objective Optimization for Structural Fatigue Test[D]. Bei Jing: Chinese Aeronautical Establishment. 2012.

[3] Zhao Hongwei. Study of Simulated Technology for Structural Fatigue testing system[D]. Bei Jing: Chinese Aeronautical Establishment. 2015.

[4] Cui Xuli, Chen Huaihai, He Xudong et al.. PID control with variable arguments for MIMO random vibration test[J]. Acta Aeronautica et Astronautica Sinica, 2010,31(9): 1776-1780.

[5] Yang Yang, Zhao Jianyu, Wang Xudong. Multi-channel synchro-loading control meyhod[J]. Journal of university of JINAN (sci & Tech), 2013,27(2): 136-139.

[6] Dong Haoran. Simulation research on hydraulic system of marine steering gear[D].Fu Jian. Jimei University.2009.

[7] Liu Xiaolin,Yuan Kun. Design and Simulation of controller for large load hydraulic loading system[J]. Control Engineering of China, 2014,21(2):210-214.

[8] Shi Zhenyun, Wang Tianmiao, Liu Da et al. A fuzzy PID-controlled SMA actuator for a two-DOF joint[J]. Chinese Journal of Aeronautics. 2014,27(2):453–460.

[9] Liu Huibo,Wang Jing,Wu Yanhe. Research and Simulation of fuzzy adaptive PID control for brushless DC motor[J]. Control Engineering of China, 2014,21(4):583-587.

[10] Yang Zhi, Chen Zhitang, Fan Zhengping et al. Tuning of PID controller based on improved partical-swarm-optimization[J]. Control Theory & Applications, 2010, 27(10): 1345-1352.

[11] Cai Jinda,Qi Jianhong. ARM9 based adaptive fuzzy PID constant cutting control system[J]. Control Engineering of China, 2014,21(3):315-320.

[12] Zhu Zhiqiang, Jiang Ziya, He Yuqing et al. Frequency properties of PID controller and model free tuning[J]. Control and Decision,2014,29(10): 1833-1838.

[13] ZHANG Haibo, WANG Jiankang, CHEN Guoqiang et al. A New Hybrid Control Scheme for an Integrated

Helicopter and Engine System[J]. Chinese Journal of Aeronautics, 2012.25(2):533-545.

[14] Yao Jianyong, Jiao Zongxia, Shang Yaoxing et al.. Adaptive Nonlinear Optimal Compensation Control for Electro-hydraulic Load Simulator[J]. Chinese Journal of Aeronautics, 2010,23(2): 720-733.

[15] Li Ke, Liu Wangkai, Wang Jun et al. An intelligent control method for a large multi-parameter environmental simulation cabin[J]. Chinese Journal of Aeronautics, 2013,26(6): 1360–1369.

[16] Zhang Zhiyong, Li Zhiqiang, Zhou Qingkun et al. Application in prestiction friction compensation for angular velocity loop of inertially stabilized platforms[J]. Chinese Journal of Aeronautics, 2014,27(3): 655–662.

[17] Wang Jin, Li Yunze , Wang Jun. Transient performance and intelligent combination control of a novel spray cooling loop system[J]. Chinese Journal of Aeronautics, 2013,26(5): 1173–1181.

[18] Zhang Deli , Yang Haiqiang, An Luling. Two-stage open-loop velocity compensating method applied to multi-mass elastic transmission system[J]. Chinese Journal of Aeronautics, 2014, 27(1): 182–188

[19] Long Yundong,Duan Xiaogang,Li Hanxiong. Study on fuzzy PID control based on time separation AFM micro cantilever[J]. Control Engineering of China, 2013,20(3):456-460.

[20] Song Zhian. MATLAB/Simulink and simulation of hydraulic control[M]. Bei Jing: National Defence Industry Press, 2012.

[21] Jelali, M., and Kroll, A. Hydraulic servo-systems: modeling, identification, and control[M]. Germany: Springer, 2003.

[22] Ye Xiaohua. Modeling and Simulation of hydraulic Spring Stiffness-based Asymmetrical Cylinder Controlled by Valve[J]. China Mechanical Engineering.2011.22(1):19-21.

[23] Jiang Hui,An Yujiao,Yuan Chaohui. Research on the flow pressure simulator of aircraft's hydraulic system[J]. Acta Aeronautica et Astronautica Sinica, 2011,32(7): 1357–1370.

[24] Li Ming-an. MATLAB/Simulink Modeling and Simulation of Dynamic Systems [M].Bei Jing: national defense industry press, 2012.

[25] Hu Shousong. Autocontrol elements[M]. Bei Jing: science press,2007.

Copyright Statement